ELSEVIER

Earth and Planetary Science Letters 208 (2003) 337–349

EPSL

www.elsevier.com/locate/epsl

Non-Arrhenian multicomponent melt viscosity: a model

Daniele Giordano *, Donald B. Dingwell

Department of Earth and Environmental Sciences, University of Munich, Theresienstr. 41/III, 80333 Munich, Germany

Received 4 September 2002; received in revised form 13 January 2003; accepted 20 January 2003

Abstract

Newtonian viscosities of 19 natural multicomponent melts ranging in composition from basanite through phonolite and trachyte, to dacite have been analysed in the range of 10^0–10^{12} Pa s. These data, together with the results of previous investigations obtained using concentric-cylinder, parallel-plate and micropenetration methods, form the basis of an analysis of multicomponent non-Arrhenian Newtonian viscosity. Regressions of the combined (high and low temperature) viscosities (ca 350 data points) were performed using the three-parameter Tammann–Vogel–Fulcher (TVF) equation:

$$\log_{10}\eta = A_{\mathrm{TVF}} + \frac{B_{\mathrm{TVF}}}{T - T_0}$$

The resulting TVF parameters were used to compose the first non-Arrhenian model for multicomponent silicate melt viscosity. The model accommodates the effects of composition via an empirical parameter, here termed the structure modifier content (SM). SM is the mol% summation of molar oxides of Ca, Mg, Mn, $Fe_{tot}/2$, Na and K. The approach is validated by the predictive capability of the viscosity model. The model reproduces the entire original dataset to within $< 10\%$ on a logarithmic scale, over 10 orders of magnitude of viscosity, 1000°C and the entire range of composition. Comparison with other empirical parameters and the Shaw model [Shaw, Am. J. Sci. 272 (1972) 870–893] is also provided.

Keywords: Newtonian; viscosity-prediction; multicomponent; silicates

1. Introduction

Magma rheology strongly controls volcanic eruptions. Thus a description of the rheology of magma is essential input for forward simulations of magmatic eruptions and for the interpretation of volcano monitoring data related to magma movements [1]. Any accurate quantification of magma rheology must, in turn, be based on a robust model for the viscosity of the liquid component, i.e. the silicate melt [2]. Due to the multicomponent nature of natural melts, the development of models for the calculation of the viscosity of multicomponent melts remains an, as yet unrealised, research goal of considerable importance.

* Corresponding author. Tel.: +49-89-2180 4250; Fax: +49-89-2180-4176.

E-mail addresses: giordano@min.uni-muenchen.de (D. Giordano), dingwell@lmu.de (D.B. Dingwell).

0012-821X/03/$ – see front matter © 2003 Elsevier Science B.V. All rights reserved.
doi:10.1016/S0012-821X(03)00042-6

Table 1a
Compositions of the investigated samples in terms of weight of the oxides; (b) on molar basis

Wt% oxides	SiO_2	Al_2O_3	FeO_{tot}	TiO_2	MnO	MgO	Cao	Na_2O	K_2O	P_2O_5	Total weight	Alkalies
HPG8 [1]	78.60	12.50	0.00	0.00	0.00	0.00	0.00	4.60	4.20	0.00	99.90	8.81
Td_ph [2]	60.46	18.81	3.31	0.56	0.20	0.36	0.67	9.76	5.45	0.06	99.64	15.27
W_ph [3]	58.82	19.42	0.00	0.79	0.00	1.87	2.35	9.31	7.44	0.00	100.00	16.75
W_T [3]	64.45	16.71	0.00	0.50	0.00	2.92	5.36	6.70	3.37	0.00	100.01	10.07
Ves_W [4]	52.02	19.28	4.65	0.59	0.14	1.72	6.58	4.53	7.69	0.65	97.82	12.49
Ves_G [4]	51.24	19.14	4.55	0.58	0.12	1.71	6.51	4.60	7.99	0.71	97.14	12.96
AMS_B1 [4]	60.10	18.03	3.43	0.38	0.14	0.73	2.92	4.49	7.89	0.16	98.27	12.61
AMS_D1 [4]	59.98	18.01	3.82	0.39	0.11	0.88	2.91	4.06	8.37	0.21	98.75	12.59
MNV [5]	63.88	17.10	2.90	0.31	0.13	0.24	1.82	5.67	6.82	0.05	98.93	12.63
ATN	59.70	18.52	3.60	0.46	0.17	0.65	2.80	3.89	8.45	0.15	98.39	12.54
PVC	63.99	16.96	2.55	0.45	0.14	0.32	0.83	6.33	6.37	0.09	98.04	12.98
UNZ	66.00	15.23	4.08	0.36	0.10	2.21	5.01	3.84	2.16	0.14	99.13	6.05
N_An [6]	61.17	17.29	5.39	0.84	0.00	3.35	5.83	3.85	1.39	0.00	99.11	5.29
Ves_G_tot	49.20	16.40	7.20	0.83	0.13	5.10	10.20	2.70	6.50	0.72	98.98	9.30
Ves_W_tot	51.20	18.60	6.10	0.67	0.13	2.50	7.30	3.75	7.90	0.40	98.55	11.82
W_Tph [7]	50.56	14.03	0.00	2.35	0.00	8.79	15.00	7.04	3.01	0.00	100.78	9.97
ETN [8]	47.03	16.28	10.13	1.61	0.20	5.17	10.47	3.75	1.94	0.59	97.18	5.85
EIF	41.15	12.10	10.11	2.74	0.00	11.24	15.66	2.76	3.04	1.02	99.82	5.81
NIQ [7]	43.57	10.18	0.00	2.97	0.00	9.17	26.07	7.59	0.96	0.00	100.51	8.51

The superscipts refer to: [1] data from [11]; [2] data from [9]; [3] data from [8]; [4] data from [14]; [5] data from [6]; [6] data from [15]; [7] data from [7]; [8] data from [5].

Table 1b
Compositions of the investigated samples on molar basis

Mol% oxides	SiO_2	Al_2O_3	FeO_{tot}	TiO_2	MnO	MgO	CaO	Na_2O	K_2O	P_2O_5	A.I.	NBO/T	SM
HPG8 [1]	84.42	7.91	0.00	0.00	0.00	0.00	0.00	4.79	2.88	0.00	0.97	0.02	7.73
Td_ph [2]	67.84	12.44	3.11	0.47	0.19	0.60	0.81	10.62	3.90	0.03	1.17	0.10	17.89
W_ph [3]	65.41	12.72	0.00	0.66	0.00	3.10	2.80	10.03	5.28	0.00	1.20	0.19	21.27
W_T [3]	69.00	10.54	0.00	0.40	0.00	4.66	6.15	6.95	2.30	0.00	0.88	0.21	20.12
Ves_W [4]	59.79	13.06	4.47	0.51	0.13	2.94	8.10	5.05	5.64	0.32	0.82	0.27	24.57
Ves_G [4]	59.42	13.08	4.41	0.50	0.12	2.95	8.08	5.17	5.91	0.35	0.85	0.28	24.81
AMS_B1 [4]	68.56	12.12	3.27	0.32	0.14	1.24	3.56	4.97	5.74	0.08	0.88	0.10	17.50
AMS_D1 [4]	68.18	12.06	3.63	0.33	0.11	1.50	3.54	4.48	6.07	0.10	0.87	0.11	17.76
MNV [5]	71.85	11.33	2.72	0.26	0.13	0.40	2.20	6.19	4.90	0.02	0.98	0.07	15.35
ATN	68.38	12.50	3.44	0.40	0.16	1.11	3.44	4.32	6.17	0.08	0.84	0.12	18.07
PVC	72.56	11.33	2.41	0.38	0.13	0.54	1.01	6.96	4.62	0.04	1.02	0.06	14.63
UNZ	71.30	9.70	3.68	0.30	0.09	3.56	5.80	4.02	1.49	0.06	0.57	0.16	17.37
N_An [6]	66.23	11.03	4.88	0.68	0.00	5.41	6.76	4.04	0.96	0.00	0.45	0.28	19.94
Ves_G_tot	55.16	10.84	4.48	0.70	0.12	8.52	12.25	2.93	4.65	0.34	0.70	0.50	31.15
Ves_W_tot	59.15	12.66	3.93	0.58	0.13	4.31	9.04	4.20	5.82	0.20	0.79	0.28	25.86
W_Tph [7]	51.32	8.39	0.00	1.79	0.00	13.30	16.31	6.93	1.95	0.00	1.06	0.86	38.53
ETN [8]	51.94	10.60	9.36	1.34	0.19	8.52	12.40	4.01	1.36	0.28	0.51	0.43	30.51
EIF	43.28	7.50	6.47	2.17	0.00	17.62	17.65	2.81	2.04	0.45	0.65	1.16	44.75
NIQ [7]	42.98	5.92	0.00	2.20	0.00	13.48	27.55	7.26	0.60	0.00	1.33	1.51	48.93

A.I. = $(Na_2O+K_2O)/Al_2O_3$; NBO/T is from Mysen [24]; SM = $\Sigma(Fe_{tot}/2+MnO+MgO+CaO+Na_2O+K_2O)$.
Molar-basis parameters are calculated assuming 'dry' the compositions with 0.02 wt% of H_2O.
The superscipts refer to: [1] data from [11]; [2] data from [9]; [3] data from [8]; [4] data from [14]; [5] data from [6]; [6] data from [15]; [7] data from [7]; [8] data from [5].

The earliest parameterisations of the viscosity of multicomponent silicate melts for geological purposes employed an Arrhenian dependence of the viscosity on temperature [3,4]. Although a useful approximation over restricted ranges of temperature, the Arrhenian approximation leads to serious errors over larger temperature ranges. In comparisons with the more complete viscosity datasets for multicomponent silicate liquids which have been coming on line in the past decade the discrepancy is repeatedly evident [5–11].

As a response to this growing evidence for the inadequacy of Arrhenian models, an empirical non-Arrhenian viscosity model for the binary system calcalkaline rhyolite–H_2O has recently been developed [10]. With that, the next natural step in the development of such models would be the extension of non-Arrhenian modelling to multicomponent melts. It has been clear for some time, however, that this step requires a substantially enlarged experimental database for its calibration and testing. A prime reason that, to date, such a model has not been forthcoming lies in the lack of a dataset complete enough to permit adequate testing of the model results. Recently, new viscosity data [5–11] have led to a change in this situation. We are now, for the first time, of the opinion that the current database (about 350 viscosity data employed here) is sufficient and covers a wide enough range of composition [5–12,15] to initiate reliable general multicomponent non-Arrhenian modelling of silicate melt viscosities. We provide herewith the first attempt.

2. Methods

The starting glasses used for the viscosity determination were prepared by fusion of total rocks or glassy matrices of the samples [12]. Next, homogenisation by stirring of the molten materials was performed at ambient pressure in the interval of 1400–1600°C until the melts were free of bubbles. Once the liquids were homogenised at high temperature, viscosities in the range of about 10^{-1}–10^{5} Pa s were determined, using a Brookfield DVIII+concentric cylinder calibrated against a DGG-1 standard glass. The temperature range of the measurements varies between 1050 and 1600°C. Viscosity was determined in steps of decreasing temperature until the minimum temperature value was reached. Possible instrumental drift was checked by reoccupying the highest temperature data point (further procedural details are found in [13]). Melt samples were then allowed to cool to room temperature. The anhydrous glass compositions were analysed by a Cameca SX50 electron microprobe, using a spot size of 20 μm and 10 nA beam current. Compositions are reported in Table 1 together with other natural and synthetic liquid compositions from previous studies [5–12,14–16] for comparison. Doubly polished 3 mm disks of the cooled glass were prepared for micropenetration viscometry as described in [11]. The oxidation state of iron may influence the viscosity of silicate melts (e.g. [17]). Nevertheless, it is demonstrated below to have little effect on the present parameterisation. On the other hand, a more accurate parameterisation of the partitioning of ferric vs ferrous iron for the

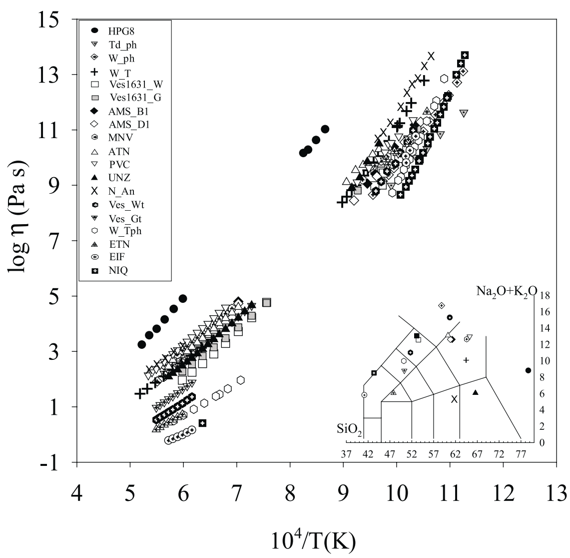

Fig. 1. Investigated viscosities and corresponding compositions. High-T (concentric cylinder) and low-T (micropenetration method) Arrhenius plots for the viscosities of the samples investigated in this work (see also [16]) and previous investigations from the literature (W_Tph and NIQ refer to [7]; W_ph and W_T refer to [8]; HPG8 refers to [10]; N_An refers to [16]). The chemical range of the investigated samples is presented according to the T.A.S. diagram (after [17]).

Table 2
Viscosity data for the dry compositions used in the modelling

Name	T (°C)	logη	Ref.
MNV	1495.50	2.50	5
MNV	1470.89	2.62	5
MNV	1446.28	2.75	5
MNV	1421.67	2.89	5
MNV	1397.06	3.03	5
MNV	1372.45	3.18	5
MNV	1347.84	3.33	5
MNV	1323.23	3.49	5
MNV	1298.62	3.65	5
MNV	1274.01	3.82	5
MNV	1249.40	3.97	5
MNV	1224.79	4.17	5
MNV	1200.18	4.36	5
MNV	1175.57	4.55	5
MNV	685.45	11.08	5
MNV	743.80	10.03	5
MNV	706.10	10.71	5
MNV	816.80	8.76	5
MNV	769.30	9.56	5
ETN	1544.72	0.18	8
ETN	1520.11	0.26	8
ETN	1495.50	0.34	8
ETN	1470.89	0.43	8
ETN	1446.28	0.52	8
ETN	1421.67	0.62	8
ETN	1397.06	0.72	8
ETN	731.63	10.23	8
ETN	711.85	10.82	8
ETN	715.85	10.70	8
Ves_G	1397.06	2.28	4
Ves_G	1347.84	2.54	4
Ves_G	1298.62	2.83	4
Ves_G	1249.40	3.15	4
Ves_G	1200.18	3.48	4
Ves_G	1150.96	3.87	4
Ves_G	1101.74	4.29	4
Ves_G	1052.52	4.75	4
Ves_G	688.95	11.05	4
Ves_G	707.25	10.66	4
Ves_G	726.70	10.20	4
Ves_G	756.35	9.78	4
Ves_G	771.15	9.58	4
Ves_G	805.10	8.81	4
Ves_W	1397.06	1.96	4
Ves_W	1347.84	2.25	4
Ves_W	1298.62	2.56	4
Ves_W	1249.40	2.91	4
Ves_W	1200.18	3.29	4
Ves_W	1150.96	3.72	4
Ves_W	1101.74	4.22	4
Ves_W	1052.52	4.77	4
Ves_W	689.20	10.68	4
Ves_W	708.50	10.26	4
Ves_W	722.95	9.97	4
Ves_W	752.25	9.44	4
Ves_W	755.12	9.01	4
Ves_W	770.00	8.98	4
Td_ph	1495.50	2.20	2
Td_ph	1470.89	2.32	2
Td_ph	1446.28	2.44	2
Td_ph	1421.67	2.57	2
Td_ph	1372.45	2.83	2
Td_ph	1347.84	2.97	2
Td_ph	1323.23	3.11	2
Td_ph	1298.62	3.26	2
Td_ph	1274.01	3.42	2
Td_ph	1249.40	3.57	2
Td_ph	1224.79	3.74	2
Td_ph	1200.18	3.91	2
Td_ph	1175.57	4.07	2
Td_ph	1150.96	4.27	2
Td_ph	1126.35	4.46	2
Td_ph	1101.74	4.65	2
Td_ph	614.71	11.63	2
Td_ph	650.81	10.85	2
Td_ph	672.74	10.32	2
Td_ph	691.64	10.00	2
Td_ph	737.26	8.99	2
VES_Gt	1544.72	0.53	
VES_Gt	1520.11	0.62	
VES_Gt	1495.50	0.71	
VES_Gt	1470.89	0.81	
VES_Gt	1446.28	0.90	
VES_Gt	1421.67	1.01	
VES_Gt	1397.06	1.12	
VES_Gt	1372.45	1.24	
VES_Gt	1347.84	1.36	
VES_Gt	696.80	10.98	
VES_Gt	707.45	10.55	
VES_Gt	720.20	10.17	
VES_Gt	729.15	9.78	
VES_Gt	744.75	9.51	
VES_Gt	756.25	9.13	
VES_Gt	766.95	8.79	
VES_Wt	1544.72	0.97	
VES_Wt	1520.11	1.07	
VES_Wt	1495.50	1.17	
VES_Wt	1470.89	1.28	
VES_Wt	1446.28	1.38	
VES_Wt	1421.67	1.50	
VES_Wt	1397.06	1.63	
VES_Wt	1372.45	1.75	
VES_Wt	1347.84	1.88	
VES_Wt	705.00	10.66	
VES_Wt	724.35	10.15	
VES_Wt	743.25	9.75	

Table 2 (*Continued*).

Name	T (°C)	logη	Ref.
W_ph	1542.35	1.92	3
W_ph	1492.85	2.12	3
W_ph	1448.75	2.33	3
W_ph	1396.25	2.57	3
W_ph	1344.25	2.86	3
W_ph	773.25	8.66	3
W_ph	761.65	8.97	3
W_ph	753.65	9.15	3
W_ph	742.05	9.38	3
W_ph	731.95	9.62	3
W_ph	716.85	9.97	3
W_ph	700.15	10.39	3
W_ph	689.35	10.67	3
W_ph	679.15	10.94	3
W_ph	668.35	11.29	3
W_ph	659.05	11.55	3
W_ph	646.85	11.96	3
W_ph	637.85	12.25	3
W_ph	625.05	12.71	3
W_ph	616.05	13.12	3
W_Tf	1445.45	0.50	7
W_Tf	1393.05	0.70	7
W_Tf	1341.25	0.91	7
W_Tf	1291.85	1.13	7
W_Tf	1240.05	1.38	7
W_Tf	1224.35	1.45	7
W_Tf	1190.35	1.65	7
W_Tf	1140.75	1.96	7
W_Tf	734.95	8.73	7
W_Tf	724.05	9.18	7
W_Tf	718.95	9.30	7
W_Tf	713.55	9.57	7
W_Tf	709.95	9.71	7
W_Tf	703.15	9.93	7
W_Tf	698.05	10.21	7
W_Tf	694.15	10.38	7
W_Tf	687.45	10.61	7
W_Tf	683.55	10.75	7
W_Tf	673.25	11.32	7
W_Tf	660.95	11.86	7
W_Tf	657.55	12.05	7
W_Tf	644.85	12.85	7
W_T	1606.45	1.64	3
W_T	1554.55	1.86	3
W_T	1503.35	2.09	3
W_T	1452.65	2.32	3
W_T	1655.55	1.46	3
W_T	1404.65	2.56	3
W_T	1355.35	2.83	3
W_T	1304.85	3.12	3
W_T	1258.55	3.41	3
W_T	840.55	8.37	3
W_T	829.95	8.58	3
W_T	818.85	8.81	3
W_T	809.45	8.99	3
W_T	792.65	9.34	3
W_T	784.05	9.53	3
W_T	771.85	9.82	3
W_T	762.95	10.04	3
W_T	741.45	10.59	3
W_T	726.05	11.09	3
W_T	725.25	11.14	3
W_T	721.05	11.23	3
W_T	708.65	11.67	3
W_T	700.15	11.96	3
W_T	677.95	12.77	3
HPG8	1642.80	3.24	1
HPG8	1593.60	3.58	1
HPG8	1544.40	3.81	1
HPG8	1495.20	4.15	1
HPG8	1446.00	4.53	1
HPG8	1396.80	4.90	1
HPG8	881.70	11.02	1
HPG8	905.00	10.63	1
HPG8	925.70	10.28	1
HPG8	938.80	10.16	1
HPG8	1180.00	6.79	1
NIQ	1300.00	0.41	7
NIQ	719.55	8.66	7
NIQ	709.75	8.94	7
NIQ	704.25	9.16	7
NIQ	698.85	9.35	7
NIQ	693.25	9.57	7
NIQ	686.35	9.88	7
NIQ	685.05	9.93	7
NIQ	679.65	10.17	7
NIQ	671.55	10.51	7
NIQ	667.75	10.75	7
NIQ	660.95	11.04	7
NIQ	656.05	11.26	7
NIQ	651.05	11.56	7
NIQ	645.55	11.83	7
NIQ	640.45	12.16	7
NIQ	638.95	12.22	7
NIQ	626.05	12.99	7
NIQ	619.15	13.40	7
NIQ	613.35	13.70	7
EIF	1470.89	−0.22	
EIF	1446.28	−0.16	
EIF	1421.67	−0.09	
EIF	1397.06	−0.02	
EIF	1372.45	0.07	
EIF	1347.84	0.16	
EIF	691.85	10.77	
EIF	702.00	10.26	
EIF	709.60	9.81	
EIF	710.00	10.05	
N_an	1593.85	2.33	6

Table 2 (*Continued*).

Name	T (°C)	logη	Ref.
N_an	1544.85	2.52	6
N_an	1494.85	2.74	6
N_an	1445.85	2.97	6
N_an	1396.85	3.19	6
N_an	763.65	10.67	6
N_an	752.35	10.90	6
N_an	738.65	11.25	6
N_an	719.05	11.83	6
N_an	707.95	12.33	6
N_an	698.65	12.64	6
N_an	688.55	12.85	6
N_an	677.45	13.30	6
N_an	666.15	13.66	6
PVC	1593.94	2.14	
PVC	1569.33	2.25	
PVC	1544.72	2.37	
PVC	1520.11	2.50	
PVC	1495.50	2.63	
PVC	1470.89	2.76	
PVC	1446.28	2.91	
PVC	1421.67	3.05	
PVC	1397.06	3.20	
PVC	1372.45	3.36	
PVC	1347.84	3.52	
PVC	1323.23	3.68	
PVC	1298.62	3.85	
PVC	1274.01	4.00	
PVC	1249.40	4.21	
PVC	1224.79	4.40	
PVC	1200.18	4.59	
PVC	722.88	10.77	
PVC	737.15	10.53	
PVC	738.59	10.41	
PVC	743.13	10.49	
PVC	749.70	10.19	
PVC	760.60	9.95	
PVC	781.80	9.63	
PVC	806.55	9.11	
ATN	1470.89	2.45	
ATN	1446.28	2.58	
ATN	1421.67	2.72	
ATN	1347.84	3.16	
ATN	1323.23	3.32	
ATN	1298.62	3.48	
ATN	1274.01	3.66	
ATN	1249.40	3.83	
ATN	1224.79	4.02	
ATN	1200.18	4.20	
ATN	1175.57	4.40	
ATN	1150.96	4.60	
ATN	761.4	10.30	
ATN	774.5	10.11	
ATN	794.3	9.73	
ATN	810.6	9.55	

Table 2 (*Continued*).

Name	T (°C)	logη	Ref.
ATN	830.9	9.11	
AMS_B1	1446.28	2.79	4
AMS_B1	1397.06	3.06	4
AMS_B1	1347.84	3.35	4
AMS_B1	1298.62	3.67	4
AMS_B1	1249.40	4.02	4
AMS_B1	1200.18	4.39	4
AMS_B1	1150.96	4.80	4
AMS_B1	693.93	11.18	4
AMS_B1	732.45	10.39	4
AMS_B1	768.25	9.41	4
AMS_B1	784.75	9.06	4
AMS_D1	1495.50	2.49	4
AMS_D1	1446.28	2.74	4
AMS_D1	1397.06	3.01	4
AMS_D1	1347.84	3.30	4
AMS_D1	1298.62	3.62	4
AMS_D1	1249.40	3.96	4
AMS_D1	1200.18	4.33	4
AMS_D1	1150.96	4.73	4
AMS_D1	683.60	11.29	4
AMS_D1	700.09	10.75	
AMS_D1	711.88	10.56	4
AMS_D1	736.40	9.77	4
AMS_D1	765.17	9.32	4
AMS_D1	813.95	8.45	4
UNZ	1470.89	2.09	
UNZ	1446.28	2.21	
UNZ	1421.67	2.34	
UNZ	1397.06	2.48	
UNZ	1372.45	2.62	
UNZ	1347.84	2.76	
UNZ	1323.23	2.92	
UNZ	1298.62	3.08	
UNZ	1274.01	3.25	
UNZ	1249.40	3.43	
UNZ	1224.79	3.61	
UNZ	1200.18	3.80	
UNZ	1175.57	4.00	
UNZ	1150.96	4.21	
UNZ	1126.35	4.44	
UNZ	1101.74	4.66	
UNZ	761.00	10.50	
UNZ	784.65	9.85	
UNZ	801.00	9.28	
UNZ	818.00	8.91	

The column 'Ref.' indicates data from literature: [1] from [11]; [2] from [9]; [3] from [8]; [4] from [14]; [5] from [6]; [6] from [15]; [7] from [7]; [8] from [5].

compositions analysed here should be obtained in future.

3. Results and TVF fitting

The data analysed for the non-Arrhenian viscosity of anhydrous multicomponent silicate melts derive from several recent investigations performed in our laboratories and further recent studies on synthetic and natural compositions [5–9,11,12,14–16]. Fig. 1 illustrates the wide range of compositions included, in terms of total alkalies versus silica [18].

Comparison of high and low viscosity data for the melts indicates (Fig. 1) that the temperature dependence of viscosity varies from slightly to strongly non-Arrhenian over the viscosity range of 10^{-1}–$10^{11.6}$ Pa s. The viscosity database for the multicomponent silicates is provided in Table 2.

Note that in the region pertinent to most magmatic processes (800–1300°C) the range is greater than six orders of magnitude of viscosity. At higher viscosities near typical glass transition temperatures the data converge such that the entire range of glass transition behaviour, as reflected by the 10^{12} Pa s isokom, is 800–600°C.

The combined viscosity results from the concentric-cylinder and micro-penetration techniques from these studies were first fit using the Tammann–Vogel–Fulcher (TVF) equation [19–21]:

$$\log_{10}\eta = A_{\mathrm{TVF}} + \frac{B_{\mathrm{TVF}}}{T - T_0} \quad (1)$$

where η is the viscosity of the melts expressed in Pa s, T is the absolute temperature, A_{TVF}, B_{TVF} and T_0 are adjustable parameters (known as the shift factor, the non-Arrhenian pseudo-activation energy and the TVF temperature, respectively). Values of the A_{TVF}, B_{TVF} and T_0 parameters were obtained for each composition and are listed in Table 3.

Table 3
Tammann–Vogel–Fulcher regression parameters

Sample	A_{TVF} (Pa s)	B_{TVF} (K)	T_0 (K)
SiO_2*	−7.26	26 984	0
HPG8[1]	−7.32	18 859	128.39
Td_ph[2]	−4.94	11 069	220.81
W_ph[3]	−3.22	7 009	458.59
W_T[3]	−3.61	7 201	510.12
Ves_W[4]	−6.76	12 183	265.80
Ves_G[4]	−6.34	11 559	304.77
AMS_B1[4]	−3.82	9 056	362.22
AMS_D1[4]	−3.86	9 108	350.20
MNV[5]	−6.05	13 654	165.02
ATN	−4.99	10 078	382.53
PVC	−5.68	13 004	205.45
UNZ	−3.63	6 879	545.14
N_an[6]	−2.97	7 184	508.67
VesGt	−4.98	6 987	531.99
VesWt	−5.05	8 070	467.16
W_Tph[7]	−3.93	4 663	639.99
ETN[8]	−4.84	6 019	602.38
EIF	−4.24	4 171	687.91
NIQ[7]	−5.06	5 289	605.55

Pre-exponential factor (A_{TVF}), pseudo-activation energy (B_{TVF}) and TVF temperature values (T_0) obtained by fitting the experimental determinations via Eq. 1. Pure SiO_2 from [20] is also included for a wider comparison.
Regression parameters are obtained using: * data from [22]; [1] data from [11]; [2] data from [9]; [3] data from [8]; [4] data from [14]; [5] data from [6]; [6] data from [15]; [7] data from [7]; [8] data from [5].

4. Composition

A central question facing any attempt to parameterise multicomponent silicate melt viscosity concerns the casting of the multicomponent chemical composition for the purpose of predicting viscosity. Much has been developed in describing the temperature, pressure and composition dependence of the structure of silicate melts and in attempts to link it to melt viscosity through structure–property models [4,23–25]. One of the most enduring aspects of melt structure models is the notion of network modifiers, whose abundance and distribution contribute to the structural description of the melt phase. In principle, all modifiers must occupy distinguishable roles and distributions within the melt phase and we might anticipate that the details of such distributions impact on melt viscosity. This clearly appears to be the case in simple silicate melt systems [26]. Nevertheless, a comparison of parameterisations based on summing interactions has been made here. This decision has been made on the empiri-

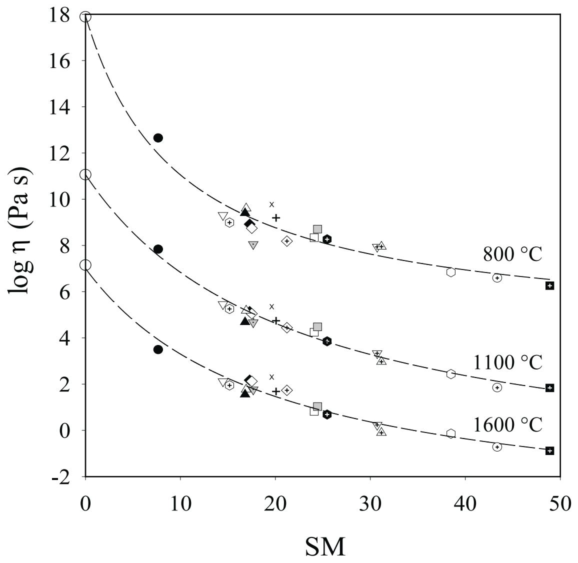

Fig. 2. Isothermal viscosities as a function of the 'structural modifier' parameter (SM). The figure reports the isothermal viscosities at $T = 800°C$ (highest curve), 1100°C and 1600°C (lowest curve). Symbols in the figure are the same as in Fig. 1. Pure SiO_2 as reported by [22] (Table 3) is also included as constituting the zero 'network modifiers' contribution.

cal basis of goodness of fit, optimising the simplicity of the parameterisation of the melt composition for the purpose of predicting viscosity. The parameterisation is based on the choice of defining the 'network modifiers' parameter (SM) as the molar oxide sum, that is SM = Σ (Na_2O+K_2O+CaO+MgO+MnO+FeO_{tot}/2). That this yields a suitable correlation between composition and the isothermal viscosities is apparent in Fig. 2. Moreover, the correlation is relatively insensitive to temperature, as the almost parallel isothermal trends shown in Fig. 2 testify. Fig. 3 shows, for comparison, the correlations between isothermal viscosity and NBO/T [24], indicating that the role of NBO/T appears less clear than that played by the parameter SM.

Expressions for the correlation between the isothermal viscosity and SM or NBO/T, respectively, were obtained for the temperature interval 700–1600°C; below 700°C there are insufficient data to warrant calibration. In fact, only five datasets (Td_ph, W_ph, N_An, W_Tph and NIQ) have a significant number of experimental points determined under 700°C. We do not, therefore, recommend extrapolations outside the temperature range 700–1600°C.

The best correlation between the isothermal viscosities and NBO/T in Fig. 3 (dashed curves) was obtained by using the following expression (Eq. 2):

$$\log_{10}\eta = a_1 + a_2 \ln(\mathrm{NBO}/T - a_3) \tag{2}$$

where a_1, a_2 and a_3 are fits to the adjustable parameters for the isothermal dataset (Table 1b).

The correlations of Fig. 2 have been fitted to hyperbolic equations of the form:

$$\log_{10}\eta = c_1 + \frac{c_2 c_3}{c_3 + \mathrm{SM}} \tag{3}$$

where the variables c_1, c_2 and c_3 represent adjustable parameters for the isothermal dataset and SM is as defined above.

The variation in fit parameters c_1, c_2 and c_3 (Eq. 3) against T(°C) are shown in Fig. 4, upper right panel. The parameters vary smoothly with T and can be predicted from the following empirical expressions:

$$c_1 = \frac{-17.80106 + 0.018708103\,T(^\circ\mathrm{C})}{1 - 2.2869\times10^{-3}\,T(^\circ\mathrm{C})} \tag{4}$$

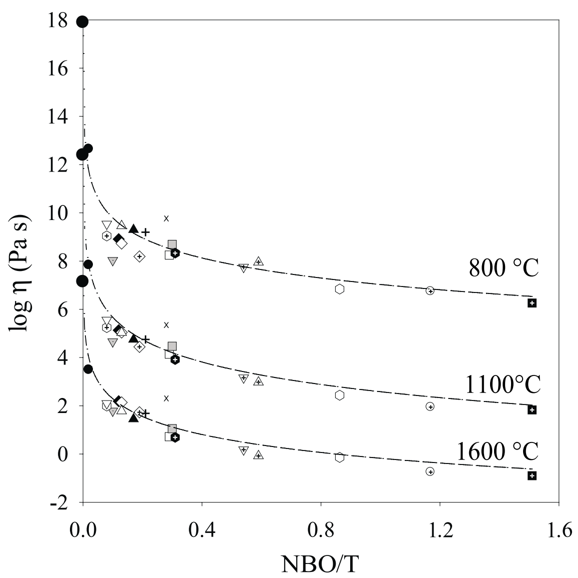

Fig. 3. Calculated isothermal viscosities versus the NBO/T ratio. The figure shows the viscosity at constant temperatures corresponding to $T = 800°C$ (highest curve), 1100°C and 1600°C (lowest curve). Symbols are the same as in Fig. 2.

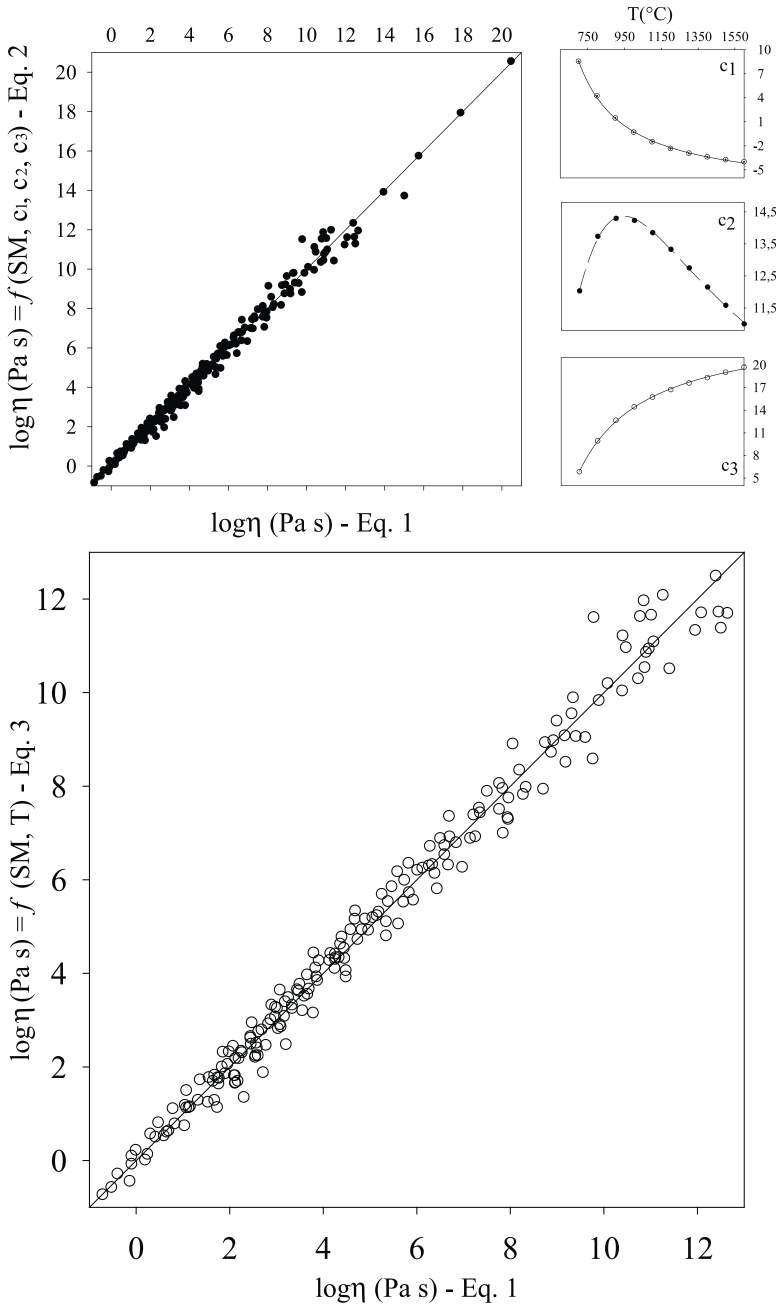

Fig. 4. Modelling steps representation and results. (Upper left panel) The viscosity calculated using Eq. 1 (which reproduces the data within a very minor error ($R^2 \sim 0.999$) with respect to the experimental determinations) versus the viscosity calculated with Eq. 2 in the temperature range 700–1600°C. (Upper right panel) The temperature dependence of the parameters c_1, c_2 and c_3 of Eq. 2. (Lower panel) Comparison between the viscosity calculated using Eq. 1 with that calculated using Eqs. 2–5, which takes into account the temperature dependence of the parameters c_1, c_2 and c_3 in the range of experimental viscosities.

$$c_2 = 0.02532 + 2.5124\exp(-6.3679\times10^{-3}T(^\circ\mathrm{C}))+ 40.4562\times10^{-6}T(^\circ\mathrm{C})^{-1} \quad (5)$$

$$c_3 = \frac{1-1.6569\times10^{-3}T(^\circ\mathrm{C})}{0.017954-63.90597\times10^{-6}T(^\circ\mathrm{C})} \quad (6)$$

The good correlation between the viscosity parameters and the compositional parameter implies two things. Firstly, the number of coefficients needed to fully describe T–logη-composition relationships is reduced from 30 (three for each isotherm) to 10, for all the measured compositions. Fig. 4, lower panel shows the comparison between the viscosities calculated using Eq. 1 and those calculated using Eqs. 2–5, for which only the compositions and the temperature are required input. Secondly, these simple empirical relationships provide a means to predict, via interpolation, the viscosity–temperature properties of other multicomponent silicate melts. The steps are summarised in Fig. 4.

Correlations with the temperature T(°C) were also fitted for the parameters a_1, a_2 and a_3 (Eq. 2) according to the following equations:

$$a_1 = -0.15139 - \frac{1129.19}{T(^\circ\mathrm{C})} - \frac{1381914}{[T(^\circ\mathrm{C})]^2} + \frac{1.29\times10^9}{[T(^\circ\mathrm{C}]^3} \quad (7)$$

$$a_2 = -0.00071 - \frac{347074}{T(^\circ\mathrm{C})} + \frac{5720.781}{[T(^\circ\mathrm{C})]^2} - \frac{2061030}{[T(^\circ\mathrm{C})]^3} \quad (8)$$

$$a_3 = -5.44516 - \frac{9309.88}{T(^\circ\mathrm{C})} - \frac{3390935}{[T(^\circ\mathrm{C})]^2} + \frac{3144300695}{[T(^\circ\mathrm{C})]^3} \quad (9)$$

Fig. 5 shows the comparison between viscosity predictions considering the parameterisations in terms of SM or NBO/T as presented here.

The different standard deviations of the fits presented here of the isothermal viscosity to the SM and the NBO/T parameters, using Eqs. 2 and 3, are 0.39 and 0.45, respectively. On the basis of this comparison, we recommend the use of the SM-based parameterisation.

Chemical parameters such as the ratios SM/(SiO_2+Al_2O_3) and SM/(100−SM) (modifiers/formers) (calculated on a molar basis) were also tried to parameterise, according to the above adopted criterion, the viscosity of silicate melts. These are not reported here as they did not provide comparably accurate predictions.

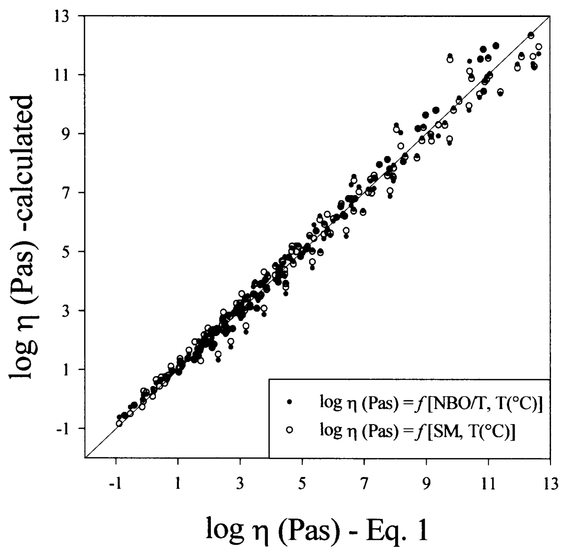

Fig. 5. Comparison between the viscosity calculated according to Eq. 1 and those calculated as a function of SM (empty circles) or NBO/T (full circles). Both parameterisations result in a good prediction of the viscosity of silicate melts. Nevertheless, a less accurate prediction is provided if the NBO/T parameter is used.

5. Discussion

An impression of how much the prediction of the present model improves the Shaw model [3] is obtained by using the three following compositions: MNV, ETN and UNZ. As seen in Table 4 the Shaw model [3] yields the largest discrepancies to the TVF interpolations of the measured viscosities. A comparison between the TVF viscosity and that calculated using Eqs. 3–6 is shown for two different assumptions regarding the proportion of the total iron in the SM parameter. Such a comparison seems to indicate that the amount of total iron and its partitioning may moderately influence the viscosity of these liquids and therefore the quality of the fit. Clearly, this matter must be dealt with in future refinements of the model.

What are we to make of the apparent success of such a simple melt composition parameter as SM,

Table 4
Comparison between the viscosity calculated by using model pertaining to Eqs. 3–6 and that from Shaw's model [3]

T (°C)	Sample	logη (Eq. 1) (Pa s)	logη (Eqs. 3–6) (Fe_{tot}) (Pa s)	logη (Eqs. 3–6) ($Fe_{tot}/2$) (Pa s)	logη (Shaw [3]) (Pa s)
1600	ETN	−0.103	−0.295	0.086	−0.004
1500		0.302	0.163	0.559	0.292
1400		0.782	0.685	1.096	0.623
1300		1.361	1.287	1.713	0.997
1200		2.073	1.987	2.425	1.421
1150		2.522	2.383	2.826	1.656
1100		2.971	2.815	3.260	1.907
1050		3.553	3.289	3.735	2.178
1000		4.135	3.816	4.258	2.470
900		5.708	5.094	5.510	3.128
800		7.950	6.935	7.289	3.909
700		11.400	10.269	10.498	4.851
		σ	0.55	0.44	2.70
1600	MNV	1.944	1.820	2.055	1.808
1500		2.441	2.368	2.615	2.246
1400		3.004	2.985	3.244	2.737
1300		3.648	3.683	3.954	3.290
1200		4.389	4.472	4.757	3.918
1150		4.821	4.906	5.197	4.265
1100		5.253	5.368	5.665	4.637
1050		5.763	5.860	6.161	5.038
1000		6.273	6.385	6.690	5.470
900		7.496	7.568	7.870	6.444
800		8.988	9.106	9.382	7.600
700		10.849	11.758	11.963	8.994
		σ	0.30	0.50	0.94
1600	UNZ	1.551	1.489	1.776	1.791
1500		1.972	2.022	2.322	2.228
1400		2.469	2.622	2.937	2.717
1300		3.063	3.302	3.631	3.268
1200		3.784	4.074	4.419	3.894
1150		4.206	4.500	4.851	4.240
1100		4.679	4.954	5.312	4.612
1050		5.213	5.441	5.803	5.011
1000		5.821	5.963	6.328	5.442
900		7.326	7.153	7.512	6.413
800		9.402	8.730	9.055	7.566
700		12.448	11.485	11.720	8.955
		σ	0.43	0.57	1.30

Two different predictions of the viscosity were attempted by considering the total iron (4th column) or its half (5th column) as network modifier. The standard deviations σ pertaining to viscosity determinations in the temperature ranges (700–1600°C) is calculated.

in comparison to NBO/T, in parameterising the multicomponent melt viscosity? We do not have a simple answer at this time. If a simple polymerisation parameter such as NBO/T leads to no improvement in the parameterisation of viscosity over the application of the SM parameter, then the qualitative conclusion must be either (a) the uncertainty in quantifying NBO/T is too large at present, or (b) the algebraic formulation of NBO/T is not directly reflecting the state of polymerisation in the melt, or (c) the state of polymerisation in the melt is not the critical factor controlling the variation of viscosity in multicomponent melts. An explanation for the last and perhaps most provocative of these theses might be worth seeking in the notion of percolation channels in silicate melts affecting their medium-range order: a notion arising from earlier spectroscopic studies [27,28] and supported by more recent molecular dynamics simulations [29,30].

6. Conclusion

The present model is provided as a step in the development of a fully generalisable description of the viscosity of geo-relevant silicate melt viscosities. Its non-Arrhenian multicomponent nature makes it an essential contribution towards that goal. It must, however, be improved and refined in a number of ways in the near future. Firstly, the present model is dry, whereas all volcanic liquids contain some water. That means that the direct application of values obtained here is restricted to processes in nature and the laboratory at ambient pressure in fully dry or degassed systems. We are certain that valuable improvements in the prediction of lava rheology in flows and fall deposits will be the short-term result of this model. Nevertheless, amongst the most important of these future steps will be the incorporation of water in the multicomponent compositional base. Secondly, the contribution of data in the intermediate viscosity region is a significant experimental challenge which should be increasingly met by centrifuge-based viscometric methods. Thirdly, and very importantly, we wish to emphasise that the assurance of complete generalisability will only be acceptable when the success of the present multicomponent parameterisation and model can be understood in structural terms with adequate structure–property relationships.

Acknowledgements

This research was supported by the International Quality Network (IQN-Exchange Program) grants. Comments by J.K. Russell are much appreciated and resulted in a clearer presentation of the paper. We would like to thank B.O. Mysen, F.J. Spera and an anonymous reviewer for the constructive reviews.***[AC]***

References

[1] D.B. Dingwell, A physical description of magma relevant to explosive silicic volcanism, in: Physics of Explosive Volcanic Eruptions, Geol. Soc. London Spec. Publ. 145, 1998, pp. 9–26.
[2] D.B. Dingwell, N.S. Bagdassarov, G.Y. Bussod, S.L. Webb, Magma rheology, in: Miner. Assoc. Canada Short Course Handbook on Experiments at High Pressures and Application to the Earth's Mantle, vol. 21, 1993, pp. 131–196.
[3] H.R. Shaw, Viscosities of magmatic silicate liquids: an empirical method of prediction, Am. J. Sci. 272 (1972) 870–893.
[4] Y. Bottinga, D. Weill, The viscosity of magmatic silicate liquids: a model for calculation, Am. J. Sci. 272 (1972) 438–475.
[5] D. Giordano, D.B. Dingwell, Viscosity of hydrous Etna basalt: implications for Plinian-style basaltic eruptions, Bull. Volcanol. 65 (2003) 8–14.
[6] D. Giordano, C. Romano, P. Papale, D.B. Dingwell, Viscosity of trachytes from Phlegrean Fields, and comparison with basaltic, phonolitic, and rhyolitic melts, J. Volcanol. Geotherm. Res. (2003) (in press).
[7] A. Whittington, P. Richet, F. Holtz, Water and the viscosity of depolymerized aluminosilicate melts, Geochim. Cosmochim. Acta 64 (2000) 3725–3736.
[8] A. Whittington, P. Richet, Y. Linard, F. Holtz, The viscosity of hydrous phonolites and trachytes, Chem. Geol. 174 (2001) 209–223.
[9] D. Giordano, D.B. Dingwell, C. Romano, Viscosity of a Teide phonolite in the welding interval, J. Volcanol. Geotherm. Res. 103 (2000) 239–245.
[10] K.U. Hess, D.B. Dingwell, Viscosities of hydrous leucogranitic melts: A non-Arrhenian model, Am. Mineral. 81 (1996) 1297–1300.
[11] D.B. Dingwell, C. Romano, K.U. Hess, The effect of water on the viscosity of a haplogranitic melt under P-T-X-conditions relevant to silicic volcanism, Contrib. Mineral. Petrol. 124 (1996) 19–28.
[12] J. Gottsmann, D. Giordano, D.B. Dingwell, Predicting shear viscosity at the glass transition during volcanic processes: a calorimetric calibration, Earth Planet. Sci. Lett. 198 (2002) 417–427.
[13] D.B. Dingwell, D. Virgo, Melt viscosities in the Na_2O-FeO-Fe_2O_3-SiO_2 system and factors controlling the relative viscosities of fully polymerized silicate melts, Geochim. Cosmoch. Acta 52 (1988) 395–403.
[14] C. Romano, D. Giordano, P. Papale, V. Mincione, D.B. Dingwell, The viscosities of hydrous melts from Vesuvius and Phlegrean Fields systems, Chem. Geol. (2003) (in press).

[15] D.R. Neuville, P. Courtial, D.B. Dingwell, P. Richet, Thermodynamic and rheological properties of rhyolite and andesite melts, Contrib. Mineral. Petrol. 113 (1993) 572–581.
[16] D. Giordano, Experimental determination and modelling of the viscosity of multicomponent natural silicate melts: volcanological implications, Doctoral Thesis, University of Munich, 2002.
[17] D.B. Dingwell, Redox viscometry of some Fe-bearing silicate liquids, Am. Mineral. 76 (1991) 1560–1562.
[18] M.J. Le Bas, R.W. Le Maitre, A. Streckeisen, R. Zanetti, A chemical classification of volcanic rocks based on the total-alkali-silica diagram, J. Petrol. 27 (1986) 745–750.
[19] D.H. Vogel, Temperaturabhängigkeitsgesetz der Viskosität von Flüssigkeiten, Phys. Z. 22 (1921) 645–646.
[20] G.S. Fulcher, Analysis of recent measurements of the viscosity of glasses, J. Am. Ceram. Soc. 8 (1925) 339–355.
[21] G. Tammann, W. Hesse, Die Abhängigkeit der Viskosität von der Temperatur bei unterkühlten Flüssigkeiten, Z. anorg. allg. Chem. 156 (1926) 245–257.
[22] M.J. Toplis, D.B. Dingwell, K.U. Hess, T. Lenci, Viscosity, fragility, and configurational entropy of melts along the join SiO_2-$NaAlSiO_4$, Am. Mineral. 82 (1997) 979–990.
[23] P. Richet, Viscosity and configurational entropy of silicate melts, Geochim. Cosmochim. Acta 48 (1984) 471–483.
[24] B.O. Mysen, Structure and Properties of Silicate Melts, Elsevier, Amsterdam 1988, 354 pp.
[25] J.F. Stebbins, P.W. McMillan, D.B. Dingwell (Eds.) Structure, Dynamics and Properties of Silicate Melts, Reviews in Mineralogy, vol 32, Mineral. Soc. America, Washington, DC, 1995.
[26] C. Romano, K.U. Hess, V. Mincione, B. Poe, D.B. Dingwell, The viscosities of hydrous $XAlSi_3O_8$ (X = Li, Na, K, $Ca_{0.5}$, $Mg_{0.5}$) melts, Chem. Geol. 174 (2001) 115–132.
[27] G.E. Brown, F. Farges, G. Calas, X-ray scattering and X-ray spectroscopy studies of silicate melts, Rev. Mineral. 32 (1995) 317–410.
[28] G.N. Greaves, K.L. Ngai, Reconciling ionic-transport properties with atomic structure in oxide glasses, Phys. Rev. B 52 (1995) 6358–6380.
[29] J. Horbach, W. Kob, K. Binder, Structural and dynamical properties of sodium silicate melts: an investigation by molecular dynamics computer simulation, Chem. Geol. 174 (2001) 87–101.
[30] A. Meyer, H. Schober, D.B. Dingwell, Structure, structural relaxation and ion diffusion in sodium disilicate melts, Eur. Lett. 59 (2002) 708–713.